Expanded palette of Nano-lanterns for real-time multicolor luminescence imaging

Akira Takai[a,1], Masahiro Nakano[b,1], Kenta Saito[b], Remi Haruno[b], Tomonobu M. Watanabe[c,d], Tatsuya Ohyanagi[e], Takashi Jin[e], Yasushi Okada[a,2], and Takeharu Nagai[b,d,f,2]

Laboratories for [a]Cell Polarity Regulation, [c]Comprehensive Bioimaging, [e]Nano-Bio Probes, and [f]Cell Dynamics Observation, Quantitative Biology Center, RIKEN, Osaka 565-0874, Japan; [b]The Institute of Scientific and Industrial Research, Osaka University, Osaka 567-0047, Japan; and [d]PRESTO, Japan Science and Technology Agency, Tokyo 102-0075, Japan

Edited by Jennifer Lippincott-Schwartz, National Institutes of Health, Bethesda, MD, and approved February 18, 2015 (received for review September 25, 2014)

Fluorescence live imaging has become an essential methodology in modern cell biology. However, fluorescence requires excitation light, which can sometimes cause potential problems, such as autofluorescence, phototoxicity, and photobleaching. Furthermore, combined with recent optogenetic tools, the light illumination can trigger their unintended activation. Because luminescence imaging does not require excitation light, it is a good candidate as an alternative imaging modality to circumvent these problems. The application of luminescence imaging, however, has been limited by the two drawbacks of existing luminescent protein probes, such as luciferases: namely, low brightness and poor color variants. Here, we report the development of bright cyan and orange luminescent proteins by extending our previous development of the bright yellowish-green luminescent protein Nano-lantern. The color change and the enhancement of brightness were both achieved by bioluminescence resonance energy transfer (BRET) from enhanced *Renilla* luciferase to a fluorescent protein. The brightness of these cyan and orange Nano-lanterns was ∼20 times brighter than wild-type *Renilla* luciferase, which allowed us to perform multicolor live imaging of intracellular submicron structures. The rapid dynamics of endosomes and peroxisomes were visualized at around 1-s temporal resolution, and the slow dynamics of focal adhesions were continuously imaged for longer than a few hours without photobleaching or photodamage. In addition, we extended the application of these multicolor Nano-lanterns to simultaneous monitoring of multiple gene expression or Ca^{2+} dynamics in different cellular compartments in a single cell.

luciferase | luminescence imaging | luminescent indicator | live imaging | bioluminescence resonance energy transfer

Live imaging with fluorescent proteins (FPs) has revolutionized modern biology. Applications of FPs have been greatly expanded by improvements in brightness and development of color variants; however, a fundamental limitation is that fluorescence requires excitation light, the power density of which is usually above 0.1 W/cm^2 for live-cell imaging. This power is comparable with direct sunshine (0.13 W/cm^2) and can sometimes cause problems, such as autofluorescence, phototoxicity, or photobleaching (1). Furthermore, to use FPs with recently developed optogenetic tools while avoiding unintended optogenetic stimulation, careful tuning of the spectrum for the stimulation and imaging has been necessary (2).

Because luminescence imaging does not depend on excitation illumination at all, it is a good candidate as an alternative imaging modality to circumvent these potential problems caused by the excitation light. However, most existing luminescent proteins (LPs) are dim because of the low enzymatic activity and the low quantum yield (QY). For example, the QY of WT *Renilla* luciferase (RLuc) is so small (3) (QY = 0.02 in this report) (Fig. S1 *A* and *B* and Table S1) that 2% of the energy derived from the oxidation of the substrate, coelenterazine, is converted into photon emission, yielding only ∼0.2 photon s^{-1} molecule^{-1} photon emission. Long exposure (typically 1–10 min with conventional luciferase) has, thus, been required, and subcellular spatial resolution has been difficult to achieve. In addition, the color variants of LPs are limited compared with those of FPs. Thus, it has been difficult to apply LP for high-speed and multicolor imaging of living cells (4).

Recently, we developed a bright yellowish-green LP called Nano-lantern (5), which is a chimera of RLuc8-S257G [an enhanced mutant (5) based on the stabilized variant called RLuc8 (3)], and Venus, a bright yellow FP with fast and efficient maturation properties (6). Three properties combined to make Nano-lantern 10 times brighter than RLuc (5), including (*i*) increased enzymatic activity of RLuc8-S257G (1.3 times higher than RLuc8), (*ii*) an optimized linker that facilitates efficient intramolecular bioluminescence resonance energy transfer (BRET) from RLuc8-S257G to Venus, and (*iii*) the high QY of Venus (QY = 0.57) (6). This enhanced brightness of Nano-lantern significantly improved the spatial and temporal resolution of luminescence imaging compared with that of conventional luciferase.

In this paper, we extend this BRET-based approach to the development of color variants of Nano-lantern by using other FPs, such as cyan and orange FPs, as the BRET acceptor. We make use of this expanded color palette of bright LPs in three proof-of-principle applications of multicolor luminescence imaging.

Significance

The application of luminescence imaging has been limited mainly by the two drawbacks of luciferases: low brightness and poor color variants. Here, we report the development of cyan and orange luminescent proteins approximately 20 times brighter than the wild-type *Renilla* luciferase. The color change and enhancement of brightness were both achieved by exploring bioluminescence resonance energy transfer (BRET) from enhanced *Renilla* luciferase to a fluorescent protein, a technology that we previously reported for the development of the bright yellowish-green luminescent protein Nano-lantern. These cyan and orange Nano-lanterns along with the original yellow Nano-lantern enable monitoring of multiple cellular events, including dynamics of subcellular structures, gene expressions, and functional status, such as intracellular Ca^{2+} change.

Author contributions: A.T., M.N., K.S., Y.O., and T.N. designed research; A.T., M.N., K.S., R.H., T.M.W., Y.O., and T.N. performed research; T.O. and T.J. contributed new reagents A.T., M.N., K.S., R.H., Y.O., and T.N. analyzed data; and A.T., M.N., Y.O., and T.N. wrote the paper.

The authors declare no conflict of interest.

This article is a PNAS Direct Submission.

Freely available online through the PNAS open access option.

Data deposition: The sequences reported in this paper have been deposited in the GenBank database (accession nos. AB982072–AB982104 and AB983214–AB983217).

[1]A.T. and M.N. contributed equally to this work.

[2]To whom correspondence may be addressed. Email: ng1@sanken.osaka-u.ac.jp or y.okada@riken.jp.

This article contains supporting information online at www.pnas.org/lookup/suppl/doi:10.1073/pnas.1418468112/-/DCSupplemental.

First, we apply the LPs as fusion tags to visualize the dynamics of subcellular microstructures, such as cytoskeletons and vesicular organelles. These submicron structures were continuously visualized at ∼1-s temporal resolution for longer than a few hours without photobleaching or photodamage. Second, an application as a multiple gene expression reporter is shown with photosensitive ES cells. Third, Ca^{2+} indicators were developed based on cyan Nano-lantern (CNL) and orange Nano-lantern (ONL), showing their usefulness as the basis for the development of luminescent indicators that are fully compatible with optogenetic tools and other optical manipulations.

Results

Development of CNL. We have first replaced Venus of the original Nano-lantern [hereafter, we call it yellow Nano-lantern (YNL)] with mTurquoise2, a cyan FP with the highest QY (QY = 0.93) among all known FPs (7) (Fig. 1*A*). The chimera of mTurquoise2-RLuc8-S257G emitted bright cyan light (Fig. 1*B*), and we named it CNL. CNL was about 20 times brighter than RLuc (Fig. 1*C*). The measured QY of CNL was similar to YNL (Table S1), which means that the higher QY of mTurquoise2 compensated for the lower spectral overlap between RLuc8 and mTurquoise2 than between RLuc8 and Venus. The nearly two times higher brightness of CNL over YNL, therefore, might reflect the higher enzymatic activity of CNL.

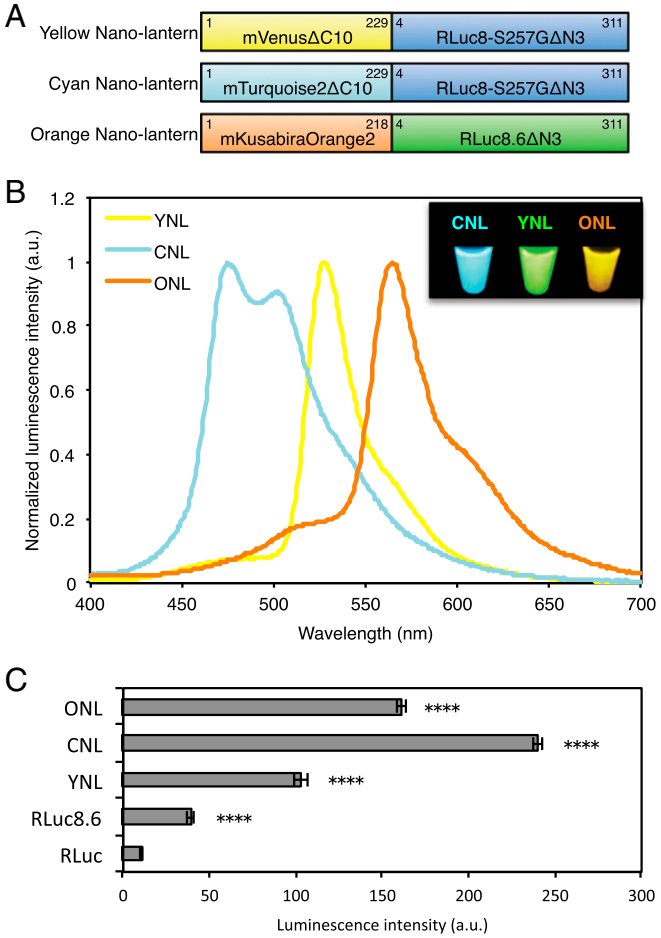

Fig. 1. Development of multicolor Nano-lanterns and their characterization. (*A*) Schematics of multicolor Nano-lanterns. Numbers represent the relative amino acid position in the original protein. (*B*) Emission spectra of LPs were measured in triplicate, and data are presented as means. (*Inset*) Luminescence of recombinant Nano-lantern proteins. (*C*) Luminescence intensities of equimolar amounts of LPs. Intensities were measured in triplicate, and data are presented as means ± SDs. One-way ANOVA followed by posthoc Tukey's honestly significant difference test compared with RLuc. ****$P < 0.0001$.

Development of ONL. We next attempted to develop a longer wavelength variant of Nano-lantern and tried various combinations of donor RLuc mutants, including long-wavelength mutants of RLuc (8), and acceptor FPs, including bright orange and red FPs (9, 10) or FPs with large Stokes shifts (11) (Figs. S2, S3, and S4). We have also tried deletions of the linker between RLuc and FP (Fig. S3). Among all of the tested constructs, the combination of RLuc8.6–535 (hereafter, RLuc8.6) and mKusabiraOrange2 (Fig. 1*A*) showed the highest BRET efficiency (Table S2). This variant emitted orange light brighter than YNL and more than 15 times brighter than RLuc (Fig. 1 *B* and *C*), and we named it ONL. For the red color variants, the combination of RLuc8.6–545 with mCherry or TurboFP635 showed relatively high BRET efficiency (Fig. S4), but additional increase of the BRET efficiency is required to use it as a fourth color combined with other Nano-lanterns. Nonetheless, these red variants will have a potential benefit for deep-tissue imaging, because absorption by tissues, especially hemoglobin, is reduced at wavelengths longer than 600 nm (12, 13).

Application as Fusion Tags for Subcellular Structures. Next, we expressed CNL and ONL as fusion proteins to examine whether they work as the luminescent fusion tags for subcellular structures (Fig. 2 and Fig. S5). Fusions with histone H2B, inositol-trisphosphate 3-kinase A (ITPKA; F-tractin) (14), β-tubulin, peroxisome targeting signal 2, zyxin, fibrillarin (Fig. 2), and all tested other various proteins or peptides (Fig. S5) showed correct localization by both fluorescence and luminescence imaging, indicating that both CNL and ONL (as well as YNL) can be used as fusion tags. Furthermore, because the emission spectrum of each color variant of Nano-lantern has a distinct peak that is distant enough from the others (Fig. 1*B*), the luminescence signals from these Nano-lantern color variants were easily separated by optical filtering (Fig. 2*B*). It should be noted that the samples were repeatedly illuminated with blue to green excitation light for CFP, YFP, or OFP excitation for fluorescence imaging. The images shown in Fig. 2 and Fig. S5 were first taken with excitation illumination (fluorescence) and then, without illumination (luminescence). Thus, our Nano-lanterns would be fully compatible with optogenetic tools.

To show live-cell imaging of subcellular structures, we examined three subcellular structures stained with ONL: lysosomes, peroxisomes, and focal adhesions (Movies S1–S3). The rapid dynamics of peroxisomes and lysosomes were examined, and their trajectories were tracked for several minutes (Fig. S6 and Movies S1 and S2), showing that the rapid dynamics of submicrometer structures can be investigated by luminescence imaging with ONL.

It should be noted that luminescence imaging is free from photobleaching and photodamage. Therefore, long-term luminescence imaging is only limited by the depletion of the substrate. Adding too much substrate coelenterazine-h, however, can increase the background luminescence because of autooxidation (15). We, therefore, synthesized diacetyl coelenterazine-h, where autooxidation is inhibited by protective acetyl groups. This inhibition of autooxidation allows diacetyl coelenterazine-h to be added at higher concentrations without increasing the background autoluminescence. Diacetyl coelenterazine-h is reverted to coelenterazine-h in the cell by esterase, which serves as a constant supply of the substrate. Thus, we can observe the luminescence signal without replenishing the substrate for several hours. With this condition, the slow dynamics of focal adhesion were observed for about 4 h continuously with 1-s exposure imaging, which is difficult with fluorescence imaging because of photobleaching (Movie S3).

Application as Gene Expression Reporters. LPs, such as firefly luciferase (FLuc), have been widely used as a reporter for gene

CELL BIOLOGY

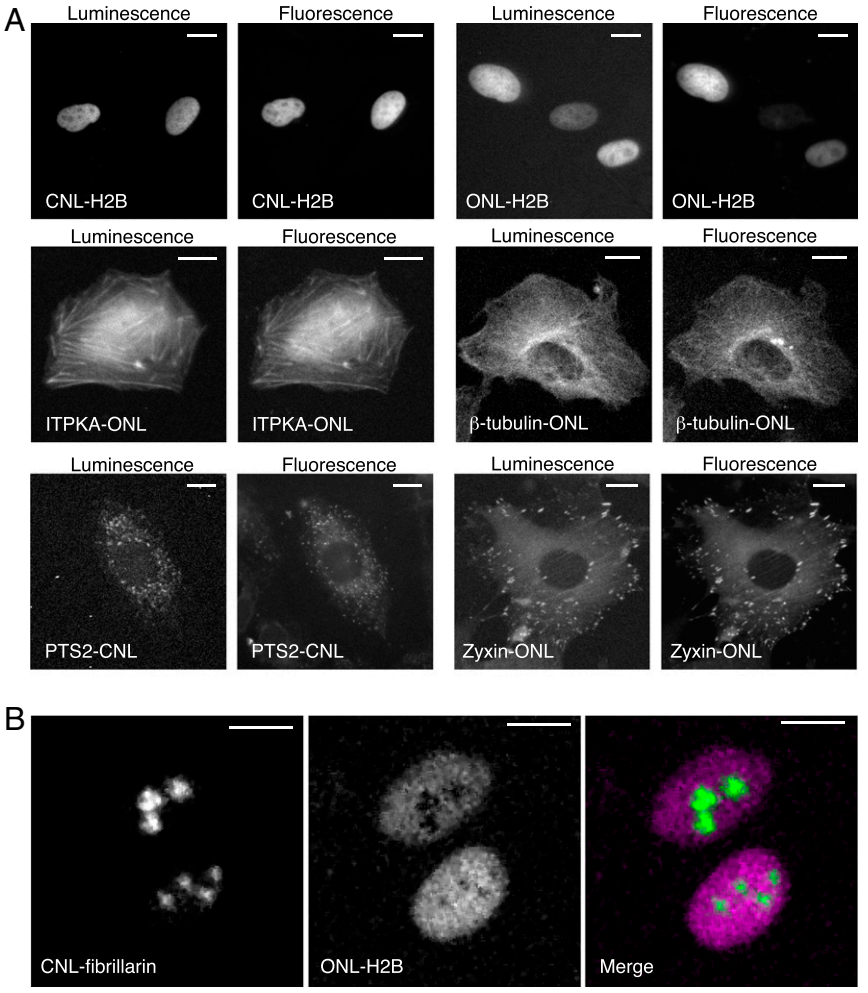

Fig. 2. Luminescence imaging of intracellular microstructures. (*A*) Luminescence and fluorescence images of subcellular structures: nuclei in interphase (CNL-H2B and ONL-H2B), F-actin [inositol trisphosphate 3-kinase A (ITPKA) -ONL], microtubules (β-tubulin-ONL), peroxisomes [peroxisome targeting signal 2 (PTS2) -CNL], and focal adhesions (zyxin-ONL). (*B*) Subnuclear structures visualized by dual-color luminescence imaging: CNL-fibrillarin (nucleoli) and ONL-H2B. Each luminescence signal was separated by linear unmixing. (Scale bars: 10 μm.)

expression with cell lysate-based assays (16, 17). However, the luminescence signal from FLuc is much weaker than that from FPs. Extremely long exposure time (1–10 min) and low spatial resolution (4 × 4 to 8 × 8 binning, resulting 2.5–5 μm/pixel) were required to collect enough photons. Thus, monitoring the dynamics of gene expression at single-cell level using FLuc has been difficult.

We, therefore, examined whether Nano-lanterns could be applied as gene expression reporters (Fig. 3 and Fig. S7). Reporter plasmids were constructed by introducing cDNA of Nano-lanterns with a nuclear localization signal (NLS) and destabilization tag (hCL1-PEST) (18) downstream of Wnt-responsive promoter 7xTcf (19). The cell line harboring this plasmid responded to Wnt-3a

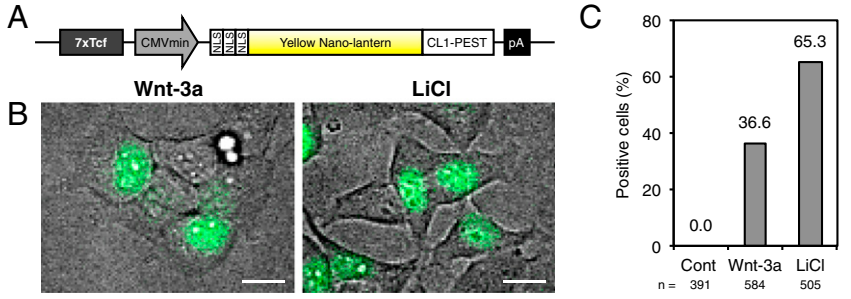

Fig. 3. Live single-cell luciferase assay for the expression of Wnt target gene. (*A*) Schematic of Nano-lantern–based Wnt signal reporter. (*B*) Luminescence of NLS-tagged Nano-lantern expressed in HEK293A cells harboring Wnt reporter construct. Images were acquired with a 495- to 540-nm band-pass emission filter at 16 h after the addition of 200 ng/mL Wnt-3a protein or 10 mM LiCl. Luminescence signals were overlaid with the bright-field image. (Scale bars: 10 μm.) (*C*) Percentages of the positive cells plotted as a bar graph. Cont, control.

as well as LiCl (Wnt signaling activator through inhibition of GSK3β). Response was sensitively detected at the single-cell level as the luminescence signal in the nucleus, even with 0.5 s of exposure time.

We next tried multiple gene expression monitoring. A stable line of murine ES cells was established, which have three gene expression reporters: *Oct4* by CNL, *Nanog* by YNL, and *Sox2* by ONL. Multichannel luminescence images of differentiating murine ES cells showed the expression level of these three genes in each cell and also, heterogeneity of the differentiation state, even within a single colony (Fig. 4). Here, imaging took only 10 s for each channel without binning (0.5 μm/pixel). This spatial resolution is high enough to distinguish single cells in a dense colony, and the temporal resolution is fast enough to monitor the dynamics of gene expression.

Application as Ca^{2+} Indicators. As another application of multicolor luminescence imaging, we constructed Ca^{2+} indicators by applying the complementation of split luciferase technology as reported previously for YNL (3). CNL- and ONL-based Ca^{2+} indicators were expressed as fusion proteins with a mitochondria localization tag and histone H2B, respectively. After stimulation with 20 μM histamine, acute Ca^{2+} spikes followed by Ca^{2+} oscillations with smaller amplitudes were observed in both mitochondria and the nucleus (Fig. 5 and Movie S4), thereby showing the same result as with FP-based Ca^{2+} indicators in a previous report (20). These results show that our multicolor Nano-lanterns could also be used as indicators for functional imaging, especially combined with optogenetic tools, such as channel rhodopsin or photoactivatable Ca^{2+} releaser (21), both of which are activated by blue light.

Discussion

Through the optimization of the BRET pairs and the linker in between them, we have succeeded in making bright cyan and orange LPs, CNL and ONL, in addition to the original YNL. The chemical energy liberated by the oxidation of the substrate coelenterazine is transferred to the FP, which emits photons with high QY. This mechanism does not only enhance the QY of luciferase but also, changes the color of the emitted light. Thus, the three color variants of Nano-lantern are about 20 times brighter than the wild-type RLuc, and their emission spectra are essentially same as those of the acceptor FPs. The enhanced brightness has enabled luminescence imaging of subcellular organelles with submicrometer and subsecond resolution. For the gene expression reporters, our proof-of-principle experiments showed that Nano-lanterns can monitor the expression of three different genes at single-cell resolution with an image acquisition time shorter than 1 min in total. Furthermore, Nano-lanterns can be applied as indicators for functional imaging, such as Ca^{2+} imaging.

Regardless of these successes, luminescence imaging with Nano-lanterns still has some drawbacks compared with fluorescence imaging with FPs. First, the signal intensity of Nano-lanterns is still more than 100 times weaker than that of FPs. A single FP molecule emits more than 1,000 photons per 1 s under conditions for single FP imaging in living cells, whereas a single Nano-lantern emits less than 10 photons per 1 s. Therefore, the application as the fusion tag for low-abundance proteins or the reporter for rapid dynamics (video rate or faster) is a remaining challenge to be overcome by additional improvements in brightness.

Second, luminescence imaging lacks optical sectioning capabilities. FPs emit signals only when illuminated with the excitation light. Thus, the signals are stronger near the focal plane with fluorescence imaging. This optical sectioning effect can be further enhanced by confocal optics, multiphoton excitation, or light-sheet illumination. Contrastingly, all of the luciferases in the sample emit signal. The signals of the thick samples are blurred by the haze from the out-of-focus luciferases.

Third, different colors of FPs can easily be separated by the combination of excitation and the emission filters. For example, a pair of FPs with emission spectrum overlap can often be separated by filtering the excitation wavelength. With luminescence imaging, the signals from different colors of Nano-lanterns can be separated only by the emission spectrum, and therefore, we have used a linear unmixing algorithm to achieve better separation (Fig. S8). Nonetheless, the unmixing algorithm can be much simpler than with fluorescence imaging, because autofluorescence signals are negligible.

Fourth, luminescence imaging requires substrate instead of excitation light. The supply and the consumption of the substrate limit the imaging. Unlike FLuc, our Nano-lanterns do not require ATP for its reaction, and therefore, the consumption of intracellular ATP does not compromise its application. However, a constant supply of the substrate coelenterazine is still necessary

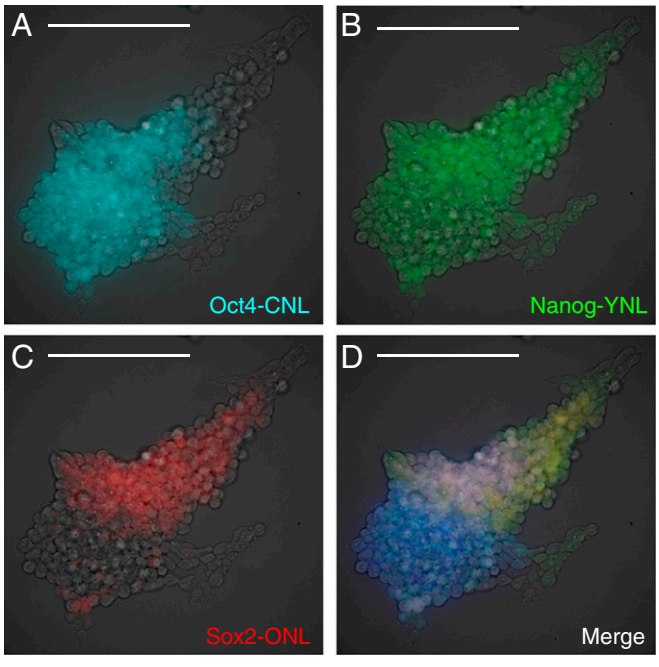

Fig. 4. Inhomogeneous expression of pluripotency markers in a single colony of ES cells. Luminescence signals of reporters for (*A*) *Oct4* (CNL), (*B*) *Nanog* (YNL), and (*C*) *Sox2* (ONL) were separated by linear unmixing and overlaid with the bright-field image. (*D*) Signals of CNL, YNL, and ONL were merged and overlaid with the bright-field image. (Scale bars: 100 μm.)

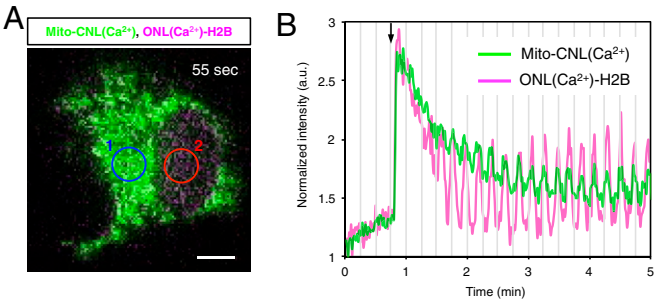

Fig. 5. Simultaneous analysis of Ca^{2+} dynamics in mitochondria and the nucleus. (*A*) Dual-channel live bioluminescence imaging of Mito-CNL(Ca^{2+}) (green) and ONL(Ca^{2+})-H2B (magenta) in HeLa cells. Dual-color luminescence image at 55 s in *B* is shown. (Scale bar: 10 μm.) (*B*) Simultaneous analysis of Ca^{2+} dynamics in the mitochondria (blue circle in *A*) and the nucleus (red circle in *A*). Arrow indicates an addition of 20 μM histamine.

CELL BIOLOGY

for stable long-term imaging. We have, therefore, synthesized diacetyl coelenterazine in this study; however, long-term imaging, especially in vivo, is still compromised by its supply. Reconstruction of synthesis or recycling of substrate would help to overcome this difficulty.

Thus, for many applications, fluorescence imaging still has many advantages over luminescence imaging. However, our three color variants of Nano-lantern are the first, to our knowledge, to enable multicolor luminescence imaging with significantly higher spatial and temporal resolution compared with conventional luciferases. Although the temporal resolution of luminescence imaging (0.1–10 s in this paper) is currently one to three orders of magnitude lower than that of fluorescence imaging (typically, 10–100 ms), the spatial resolution achieved here is comparable with cultured cells (Fig. 2 and Fig. S5). Our proof-of-principle experiments reported in this paper clearly show that luminescence imaging has become a practical alternative when the side effects by the excitation light are not negligible, such as when the samples are very sensitive to photodamage. The combination with optogenetic tools would be the most effective future application of luminescence imaging, because the external light illumination can be reserved for optical stimulation.

Materials and Methods

General. DNA oligonucleotides used for gene cloning and construction were purchased from Invitrogen or Greiner. KOD-plus-Neo (TOYOBO) was used for PCR. Products of PCR and restriction enzyme digestion were purified by agarose gel electrophoresis followed by the FastGene Gel/PCR Extraction Kit (Nippon Genetics). Restriction enzymes were purchased from New England Biolabs, and the ligase was purchased from TOYOBO (Ligation high version 2) and used as recommended by the manufacturer. Plasmids were prepared from the bacterial liquid culture by using either the Fast-n-Easy Plasmid Mini-Prep Kit (Jena Bioscience) or NucleoBond Xtra Midi Plus (Machery-Nagel). The DNA sequences were read by dye terminator cycle sequencing using the BigDye Terminator v3.1 Cycle Sequencing Kit (Life Technologies). Other reagents, such as buffer salts, were purchased from Wako.

Construction of Color Variants of Nano-Lantern. Unless stated otherwise, we used the term RLuc8.6 as RLuc8.6–535. Based on the design of the original YNL, cDNA of FPs with or without C-terminal extra amino acids for β-barrel of FPs was PCR-amplified, and cDNA of Venus in pcDNA3-YNL was replaced by the PCR products. Actual amino acid sequences used in this study were mTurquoise2 (1–229 aa), mKusabiraOrange2 (1–218 aa), LSS-mOrange (1–236 aa for FL and 1–226 aa for ΔC10), mKeima-Red (1–218 aa), tdTomato (1–464 aa), mCherry (1–226 aa), TurboFP635 (1–225 aa), mKate2 (1–222 aa), mOrange2 (1–226 aa), TagRFP (1–225 aa), mRuby2 (1–225 aa), and TurboFP650 (1–224 aa). The cDNA of TurboFP650 was generated by PCR-based mutagenesis using cDNA of TurboFP635 as a PCR template. For RLuc8.6- and RLuc8.6–545-based BRET constructs, cDNA of RLuc8.6 and RLuc8.6–545 without N-terminal 3 aa (RLuc8.6ΔN3 and RLuc545ΔN3, respectively) was generated by PCR-based mutagenesis using cDNA of RLuc8 as a PCR template, and cDNA of RLuc8-S257GΔN3 in pcDNA3-YNL was replaced by these PCR products.

Construction of Gene Expression Reporter Genes and Ca^{2+} Indicators. Wnt-responsive enhancer 7xTcf and CMV minimal promoter were PCR-amplified and subcloned into modified pT2-UAS-MCS vector (22) after the removal of UAS to obtain pT2-7xTcf-MCS. In addition, PGK promoter and puromycin resistance gene were PCR-amplified and subcloned into the vector to obtain pT2-7xTcf-MCS-PGK-Puro. For the construction of pT2-7xTcf-NLS-Nano-lanterns, cDNA of NLS-Nano-lanterns was subcloned into pT2-7xTcf-MCS-PGK-Puro vector. For the construction of pT2-7xTcf-NLS-YNL-CP, cDNA of the hCL1-PEST sequence was generated by the synthesized DNA oligonucleotides and PCR amplification and ligated to the C terminus of NLS-YNL of pT2-7xTcf-NLS-YNL.

Transcriptional promoter reporters to mouse *Nanog*, *Oct4*, or *Sox2* activity were built based on lentivirus vector to mouse *Nanog*, *Oct4*, or *Sox2* activity (23). We purchased the plasmid of Mouse Nanog Differentiation Reporter (System Biosciences), which is a commercialized lentivector-based reporter with Nanog promoter, and replaced the cDNA of RFP in the plasmid with that of YNL. The *Oct4*-CNL reporter plasmid was constructed from this Nanog-YNL plasmid by replacing the promoter with *Oct4* and the reporter with CNL. The *Sox2*-ONL reporter plasmid was similarly constructed from pGreenFire1-mCMV (System Biosciences) by replacing minimal CMV promoter and copGFP cDNA with the *Sox2* promoter and ONL cDNA, respectively.

Based on the design of Nano-lantern (Ca^{2+}), we constructed Ca^{2+} indicators of CNL and ONL [CNL(Ca^{2+}) and ONL(Ca^{2+}), respectively] by inserting a cDNA fragment encoding the CaM-M13 peptide derived from the Nano-lantern (Ca^{2+}) at the site between 228 and 229 aa of the RLuc variants in CNL and ONL.

ACKNOWLEDGMENTS. We thank the following people for the plasmids: J. Goedhart and T. W. J. Gadella (University of Amsterdam) for mTurquoise2; A. Miyawaki (RIKEN) for mKusabiraOrange2; D. M. Scherbakova and V. Verkhusha (Albert Einstein College of Medicine) for LSSmOrange; M. Z. Lin (Stanford University) for mRuby2 (Addgene Plasmid 40260); K. Kawakami for Tol2; and S. Niwa and N. Hirokawa (University of Tokyo) for β-tubulin and Rab11a. We also thank the laboratory members, especially S. Xu, J. Asada, M. Komeno and M. Kakiuchi (Quantitative Biology Center) and K. Sakai (Osaka University) for their technical and secretarial assistance and D. Priest (Quantitative Biology Center) for editing the manuscript. Part of this work was supported by KAKENHI Grants-in-Aid for Scientific Research 25871128 (to A.T.), 24659092 (to Y.O.), 25113723 (to Y.O.), and 25293046 (to Y.O.); RIKEN Incentive Research Grant (to A.T.); Ministry of Education, Science, Sports and Culture Grants-in-Aid for Scientific Research on Innovative Areas "Spying minority in biological phenomena (no. 3306)" 26115721 (to Y.O.) and 23115003 (to T.N.); and the Strategic Programs for R&D (President's Discretionary Fund) of RIKEN (Y.O.), Precursory Research for Embryonic Science and Technology (T.N.), and Development of Systems and Technology for Advanced Measurement and Analysis (T.N.) from Japan Science and Technology Agency.

1. Magidson V, Khodjakov A (2013) Circumventing photodamage in live-cell microscopy. *Methods Cell Biol* 114:545–560.
2. Akerboom J, et al. (2013) Genetically encoded calcium indicators for multi-color neural activity imaging and combination with optogenetics. *Front Mol Neurosci* 6:2.
3. Loening AM, Fenn TD, Wu AM, Gambhir SS (2006) Consensus guided mutagenesis of Renilla luciferase yields enhanced stability and light output. *Protein Eng Des Sel* 19(9):391–400.
4. Miyawaki A (2007) Bringing bioluminescence into the picture. *Nat Methods* 4(8): 616–617.
5. Saito K, et al. (2012) Luminescent proteins for high-speed single-cell and whole-body imaging. *Nat Commun* 3:1262.
6. Nagai T, et al. (2002) A variant of yellow fluorescent protein with fast and efficient maturation for cell-biological applications. *Nat Biotechnol* 20(1):87–90.
7. Goedhart J, et al. (2012) Structure-guided evolution of cyan fluorescent proteins towards a quantum yield of 93%. *Nat Commun* 3:751.
8. Loening AM, Wu AM, Gambhir SS (2007) Red-shifted Renilla reniformis luciferase variants for imaging in living subjects. *Nat Methods* 4(8):641–643.
9. Sakaue-Sawano A, et al. (2008) Visualizing spatiotemporal dynamics of multicellular cell-cycle progression. *Cell* 132(3):487–498.
10. Miranda JG, et al. (2012) New alternately colored FRET sensors for simultaneous monitoring of Zn^{2+} in multiple cellular locations. *PLoS ONE* 7(11):e49371.
11. Shcherbakova DM, Hink MA, Joosen L, Gadella TWJ, Verkhusha VV (2012) An orange fluorescent protein with a large Stokes shift for single-excitation multicolor FCCS and FRET imaging. *J Am Chem Soc* 134(18):7913–7923.
12. Dragulescu-Andrasi A, Chan CT, De A, Massoud TF, Gambhir SS (2011) Bioluminescence resonance energy transfer (BRET) imaging of protein-protein interactions within deep tissues of living subjects. *Proc Natl Acad Sci USA* 108(29):12060–12065.
13. Chu J, et al. (2014) Non-invasive intravital imaging of cellular differentiation with a bright red-excitable fluorescent protein. *Nat Methods* 11(5):572–578.
14. Johnson HW, Schell MJ (2009) Neuronal IP3 3-kinase is an F-actin-bundling protein: Role in dendritic targeting and regulation of spine morphology. *Mol Biol Cell* 20(24):5166–5180.
15. Zhao H, et al. (2004) Characterization of coelenterazine analogs for measurements of Renilla luciferase activity in live cells and living animals. *Mol Imaging* 3(1):43–54.
16. Takai A, et al. (2010) Anterior neural development requires Del1, a matrix-associated protein that attenuates canonical Wnt signaling via the Ror2 pathway. *Development* 137(19):3293–3302.
17. Balaskas N, et al. (2012) Gene regulatory logic for reading the Sonic Hedgehog signaling gradient in the vertebrate neural tube. *Cell* 148(1-2):273–284.
18. Metzger MB, Maurer MJ, Dancy BM, Michaelis S (2008) Degradation of a cytosolic protein requires endoplasmic reticulum-associated degradation machinery. *J Biol Chem* 283(47):32302–32316.
19. Fuerer C, Nusse R (2010) Lentiviral vectors to probe and manipulate the Wnt signaling pathway. *PLoS ONE* 5(2):e9370.
20. Nagai T, Sawano A, Park ES, Miyawaki A (2001) Circularly permuted green fluorescent proteins engineered to sense Ca^{2+}. *Proc Natl Acad Sci USA* 98(6):3197–3202.
21. Fukuda N, Matsuda T, Nagai T (2014) Optical control of the Ca^{2+} concentration in a live specimen with a genetically encoded Ca^{2+}-releasing molecular tool. *ACS Chem Biol* 9(5):1197–1203.
22. Kawakami K, et al. (2004) A transposon-mediated gene trap approach identifies developmentally regulated genes in zebrafish. *Dev Cell* 7:133–144.
23. Hotta A, et al. (2009) Isolation of human iPS cells using EOS lentiviral vectors to select for pluripotency. *Nat Methods* 6(5):370–376.

Supporting Information

Takai et al. 10.1073/pnas.1418468112

SI Materials and Methods

Synthesis of Coelenterazine-h and Diacetyl Coelenterazine-h. Coelenterazine-h was synthesized as reported previously (1–4). Diacetyl coelenterazine-h was synthesized as follows. Coelenterazine-h (50 mg, 0.13 mmol) in pyridine (4 mL) was mixed with acetic anhydride (2 mL) and stirred at room temperature for 2 h. The reaction mixture was concentrated in vacuo and purified by silica gel column chromatography (hexane:EtOAc = 1:9; then, EtOAc:EtOH = 2:1) to give diacetyl coelenterazine-h [48.4 mg, 80% (wt/wt)] as a yellow solid powder. ^{1}H-NMR (400 MHz, DMSO-d6, 298 K) δ = 2.31 (s, 3H), 2.37 (s, 3H), 4.09 (s, 2H), 4.47 (s, 2H), 7.23–7.29 (m, 12H), 7.46 (dd, J = 1.2 Hz, 2H), 8.07 (d, J = 6.8 Hz, 2H), and 8.70 (s, 1H). MS [electrospray ionization (ESI); mass to charge ratio] calculated for $C_{30}H_{26}N_3O_4^+$, [M^+]: 492.19; found: 492.19.

Construction of Fusion Genes. cDNA of Nano-lanterns was PCR-amplified with 5′ primers encoding an NheI site and 3′ primers encoding a BspEI site without termination codons. The PCR products were ligated into similarly digested pEGFP-C1 cloning vector to create pYNL-C1, pCNL-C1, and pONL-C1 (C1 vectors for Nano-lanterns). In the same way, pYNL-N1, pCNL-N1, and pONL-N1 (N1 vectors for Nano-lanterns) were constructed with 5′ primers encoding an AgeI site, 3′ primers encoding an NotI site, and pEGFP-N1 cloning vector. cDNA of each protein domain was PCR-amplified with primers containing the appropriate restriction sites and ligated into C1 or N1 vectors for Nano-lanterns. To prepare N-terminal fusions to Nano-lanterns, the following digests were performed: the mitochondrial targeting sequence from subunit VIII of human cytochrome *c* oxidase, NheI and BamHI; three copies of NLS of the simian virus 40 large T antigen, NheI and BamHI; the peroxisomal targeting signal 2, EcoRI and SalI; mouse β-tubulin class V (TUBB5), EcoRI and SalI; human zyxin, EcoRI and SalI; rat LAMP1, EcoRI and BamHI; human 9–52 aa of rat inositol trisphosphate 3-kinase A, HindIII and BamHI; and chicken vinculin, EcoRI and SalI. To prepare C-terminal fusions to Nano-lanterns, the following digests were performed: human RhoB GTPase, EcoRI and SalI; the PTS1 (the tripeptide SKL), EcoRI and SalI; human histone H2B, EcoRI and SalI; human Rab11a, EcoRI and SalI; and human fibrillarin, EcoRI and SalI.

Protein Purification and Characterization. LPs with 6xHis tags at their N termini were expressed from modified pET vectors in *Escherichia coli* strain BL21(DE3)-RIL (Agilent Technologies) as reported previously (5). In short, transformants were cultured in phosphate-buffered 2.5× yeast extract and tryptone (YT) medium at 37 °C until OD reached 1.0 followed by the induction of protein expression with 0.1 mM isopropyl β-D-thiogalactopyranoside (IPTG) for 24 h at 24 °C. The bacterial cells were collected and lysed with lysozyme. The lysate was clarified by centrifugation and applied to an immobilized metal affinity chromatography column TALON (Clontech). The peak elution fraction was further purified with a gel filtration column Superdex 200 (GE Healthcare) followed by the final purification with the anion exchange column Mono Q (GE Healthcare). Protein concentrations were measured with Coomassie Plus Protein Assay Reagent (Pierce) using BSA as the standard and diluted with Hepes buffer of 50 mM Hepes (pH 7.2) and 0.01% casein.

Luminescence intensities were measured in triplicate with a multiplate reader MTP-880Lab (Corona Electric). The concentrations of LPs and coelenterazine-h are final 10 pM and final 0.741 μM, respectively, and average luminescence intensities for the initial 10 s are presented in Fig. 1*C*.

The luminescence QYs were estimated from the total light output by the complete consumption of 0.2 picomole of coelenterazine-h (Fig. S1 *A* and *B*). The photon sensitivity of the detector was calibrated with the luminol chemiluminescence as reported (6). The final concentrations of LPs and coelenterazine-h were 12.5 and 2 nM, respectively.

The kinetic parameters were measured from the reactions of final 10 pM LPs with final 0.0823, 0.247, 0.741, 2.22, 6.66, 20.0, and 60.0 μM coelenterazine-h (Fig. S1 *C* and *D*). The initial reaction velocities were measured as the integrated luminescence intensities for the initial 10 s. Michaelis–Menten constant (K_m) and maximum reaction velocity (V_{max}) were estimated from the nonlinear fitting to the Michaelis–Menten equation using the Levenberg–Marquardt method implemented in the free software SciDAVis.

For measurement of emission spectra of recombinant proteins (Fig. 1*B*), proteins and coelenterazine-h were diluted with Hepes buffer and analyzed with a photonic multichannel analyzer PMA-12 (Hamamatsu) at room temperature using 200-ms exposures and 40-times averaging. The final concentrations of proteins and coelenterazine-h were 20 nM and 20 μM, respectively.

For the screening for BRET constructs, crude lysates of MDCKII expressing each BRET protein (Fig. S3) or partially purified recombinant protein from *E. coli* (Figs. S2 and S4) were used. The crude lysates of MDCKII cells were prepared by the cell lysis for 15 min at 4 °C with the following buffer: 50 mM Tris·HCl, pH 7.5, 150 mM NaCl, 1% Nonidet P-40, and 1 mM PMSF. The lysates were clarified before use. The partially purified recombinant proteins were prepared by the immobilized metal affinity chromatography with TALON from the bacterial lysate.

Cell Culture. MDCKII, HEK293A, and HeLa cells were cultured in DMEM containing 10% (vol/vol) FBS. Cells were transfected with Transfectin (Bio-Rad) according to the manufacturer's protocol. For the establishment of stable Wnt reporter lines of HEK293A cells, Wnt reporter constructs were transduced into HEK293A cells using the Tol2 transposon system (7). In short, cells were transfected with the expression plasmid of Tol2 transposase (pCS-TP) and Wnt reporter plasmids carrying Tol2 transposable elements and selected with the addition of 10 μg/mL puromycin in the culture medium at 1 wk after the transfection. Single colonies were picked up around 3 wk after the transfection, expanded, and subjected to additional analysis.

Murine ES cells (mESCs; E14Tg2a) were maintained using DMEM (Sigma) containing 10% (vol/vol) FBS, 1% penicillin (Sigma), 1% streptomycin (Sigma), 1% GlutaMAX-1 (Gibco), 1% nonessential amino acid (Gibco), 1% nucleosides (Millipore), 1% sodium pyruvate (Sigma), 0.1 mM 2-mercaptoethanol (Sigma), and 0.1% leukemia inhibitory factor (Nacalai). mESCs were cultured on 0.1% gelatin (Millipore) -coated 10-cm dishes (BD Bioscience). The reporter genes were transduced into mESCs with lentivirus produced in HEK293T cells. The infected mESCs were sorted with FACS Aria (BD Bioscience), expanded, and subjected to additional analysis.

Luminescence Imaging. For the luminescence image of recombinant multicolor Nano-lantern proteins (Fig. 1*B*, *Inset*), 100 μM coelenterazine-h was mixed with crude recombinant proteins. The picture was taken with RICOH's compact digital camera CX1.

Luminescence images of subcellular structures (Fig. 2, Figs. S5 and S6, and Movies S1–S3) were acquired with an inverted microscope IX81 (Olympus) using an objective lens UApo 40×/1.35 (Olympus) and an electron multiplying charge coupled device (EMCCD) camera iXon3 897 (Andor). Gene expression was monitored (Fig. 3 and Fig. S7) by using an LV200 Bioluminescence Microscope (Olympus). MDCKII and HeLa cells were cultured on a 35-mm glass-bottomed dish (MatTek). For HEK293A cells and mESCs, cells were cultured on 35-mm glass-bottomed dishes coated with matrigel (BD Biosciences) and collagen I (IWAKI), respectively. The culture media were exchanged to HBSS(+) (Wako) supplemented with 60 μM coelenterazine-h. Exposure times were 0.5 (Fig. 3*B*) and 10 s (Fig. 4).

For the dual-color luminescence imaging of Nano-lantern–based Ca^{2+} indicators (Fig. 5), images were acquired with W-View (Hamamatsu) equipped with 550-nm short- and long-pass filters. Images were recorded at 1 Hz (1 frame per 1 s), and final concentrations of coelenterazine-h and histamine were both 20 μM.

For long-time luminescence imaging (Movies S1–S3), 100 μM diacetyl coelenterazine-h was used as the substrate to reduce autoluminescence by autooxidation in culture medium. To prepare the solution of diacetyl coelenterazine-h, the substrate was dissolved in DMSO, mixed with an equal volume of pluronic F-127 [20% (wt/vol) DMSO solution; Biotium], and diluted with culture medium.

Multicolor Imaging with Linear Unmixing. For the multicolor luminescence imaging, four images were acquired with 460- to 510-nm band-pass (for CNL signal), 495- to 540-nm band-pass (CNL + YNL), 540-nm long-pass (YNL + ONL), and 575- to 625-nm band-pass (ONL) filters (Semrock). Three ES cell lines (each expressing Oct4-CNL, Nanog-YNL, or Sox2-ONL) were imaged with the same conditions (Fig. S8*A*) to determine the coefficients for linear unmixing (Fig. S8*B*). The signals from CNL, YNL, and ONL were then separated by linear unmixing (Fig. S8*C*) using these coefficients by an open-source software ImageJ (8).

Luciferase Assay. For the luciferase assays in Fig. S7 *F*–*I*, stable Wnt reporter lines of HEK293A were cultured in a gelatin-coated 96-well black microplate (Thermo) at the concentration of 30,000 cells per well with or without 10 mM LiCl. The luminescent intensities were measured with 10 μM coelenterazine-h at 16 h after the seeding.

Data Analysis and Statistical Methods. For trajectory analysis (Fig. S6 *C* and *D*), the positions of lysosomes and peroxisomes were determined by a 2D Gaussian fitting algorithm with custom software (9). For statistical analysis, we used the R software. Two- and multiple-group analyses were performed with Student's *t* test and one-way ANOVA followed by posthoc Tukey's honestly significant difference test, respectively.

1. Jiang B, Yang CG, Xiong WN, Wang J (2001) Synthesis and cytotoxicity evaluation of novel indolylpyrimidines and indolylpyrazines as potential antitumor agents. *Bioorg Med Chem* 9(5):1149–1154.
2. Adamczyk M, et al. (2003) Synthesis of 3,7-dihydroimidazo[1,2a]pyrazine-3-ones and their chemiluminescent properties. *Tetrahedron* 59(41):8129–8142.
3. Mori K, Maki S, Niwa H, Ikeda H, Hirano T (2006) Real light emitter in the bioluminescence of the calcium-activated photoproteins aequorin and obelin: Light emission from the singlet-excited state of coelenteramide phenolate anion in a contact ion pair. *Tetrahedron* 62(26):6272–6288.
4. Levi J, De A, Cheng Z, Gambhir SS (2007) Bisdeoxycoelenterazine derivatives for improvement of bioluminescence resonance energy transfer assays. *J Am Chem Soc* 129(39):11900–11901.
5. Okada Y, Hirokawa N (1999) A processive single-headed motor: Kinesin superfamily protein KIF1A. *Science* 283(5405):1152–1157.
6. Ando Y, et al. (2007) Development of a quantitative bio/chemiluminescence spectrometer determining quantum yields: Re-examination of the aqueous luminol chemiluminescence standard. *Photochem Photobiol* 83(5):1205–1210.
7. Urasaki A, Morvan G, Kawakami K (2006) Functional dissection of the Tol2 transposable element identified the minimal cis-sequence and a highly repetitive sequence in the subterminal region essential for transposition. *Genetics* 174:639–649.
8. Schneider CA, Rasband WS, Eliceiri KW (2012) NIH Image to ImageJ: 25 years of image analysis. *Nat Methods* 9(7):671–675.
9. Furuta K, Toyoshima YY (2008) Minus-end-directed motor Ncd exhibits processive movement that is enhanced by microtubule bundling in vitro. *Curr Biol* 18(2):152–157.

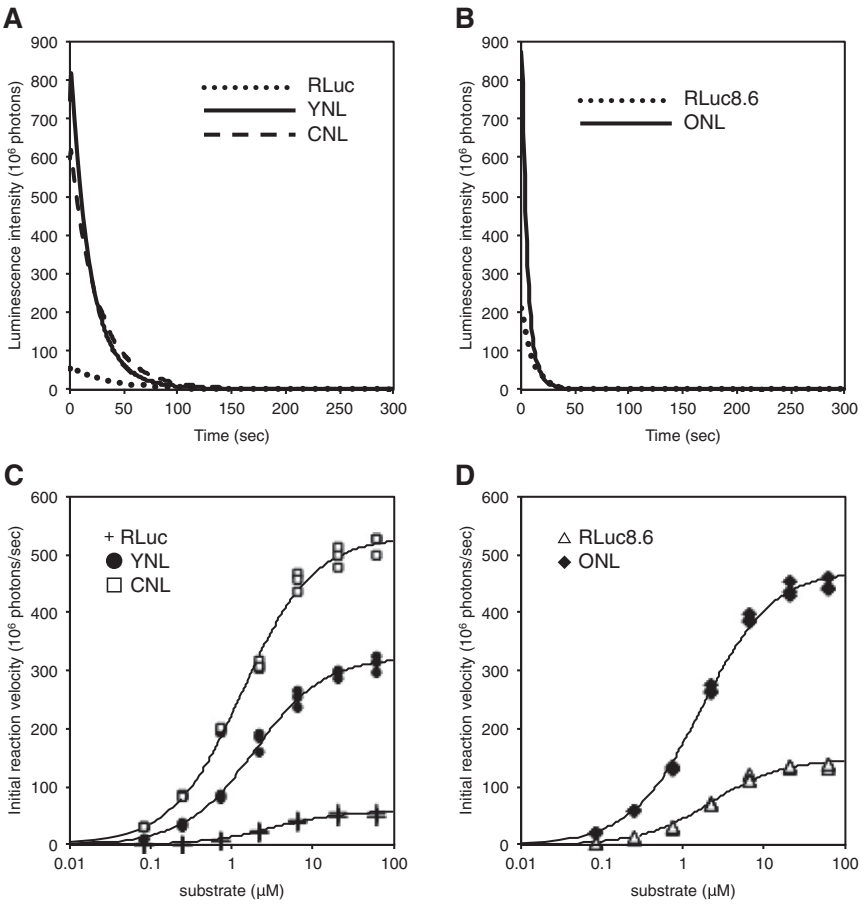

Fig. S1. Characterization of LPs. (*A* and *B*) QY was estimated from the integrated light output for 5 min until the reaction of 2 nM coelenterazine-h with 12.5 nM LP approached completion. Intensities were measured in triplicate, and data are presented as means. The results are summarized in Table S1. (*C* and *D*) Kinetics parameters were estimated from the plot of the initial light output (first 10-s integration) vs. the concentration of the substrate, coelenterazine-h. All intensities were measured in triplicate, and the average data were fitted to the Michaelis–Menten equation. The results are summarized in Table S1.

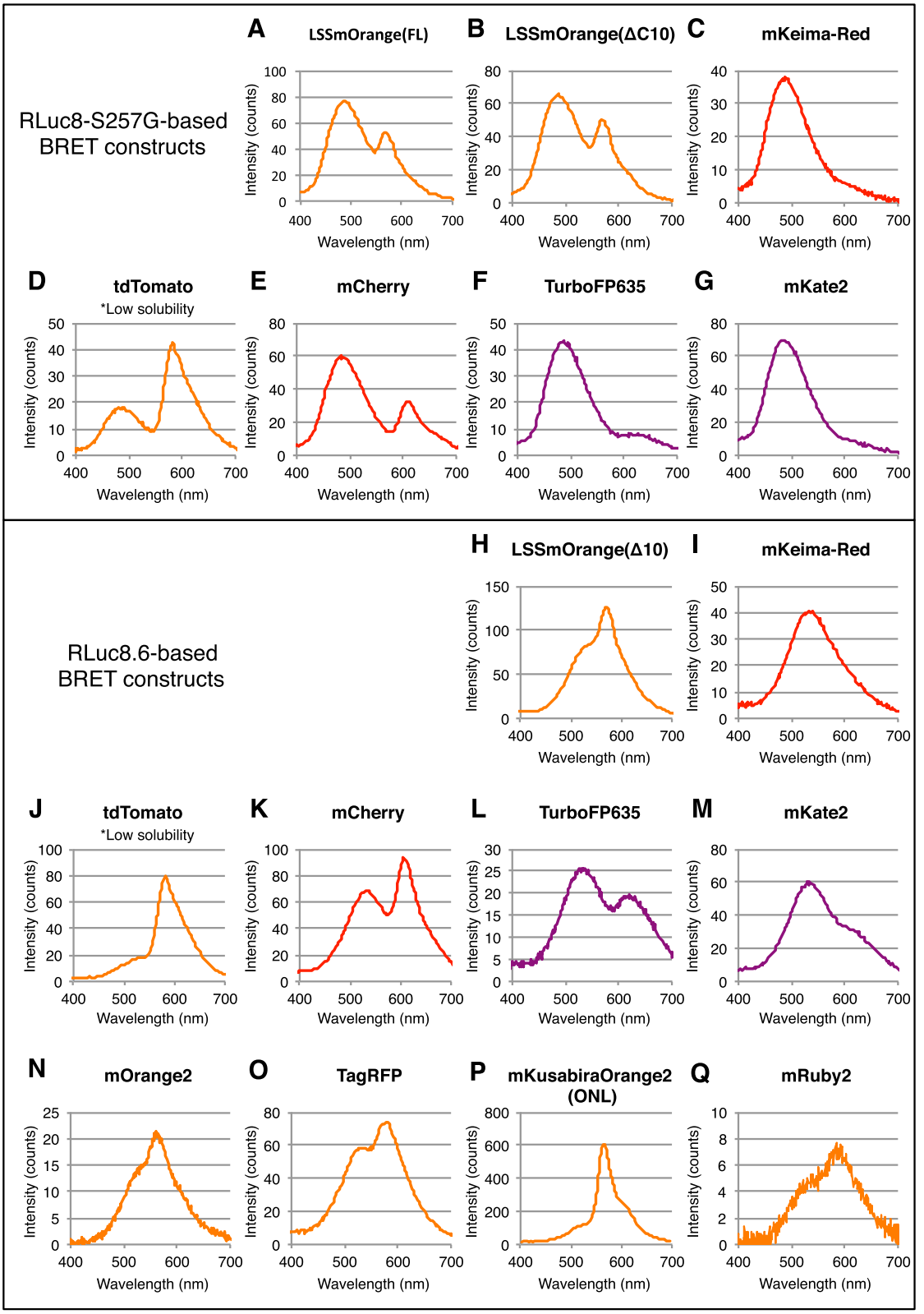

Fig. S2. Emission spectra of BRET proteins based on the design of Nano-lantern. (*A–G*) Emission spectra of BRET proteins based on RLuc8-S257G(ΔN3), the donor of YNL. Except for LSSmOrange(FL), C-terminal amino acids of FPs were deleted at the last amino acid of each β-barrel. In the case of LSSmOrange(FL), no C-terminal amino acids were deleted. In the case of tdTomato, most of BRET protein was insoluble. (*H–Q*) Emission spectra of BRET proteins based on RLuc8.6 (ΔN3), the donor of ONL. BRET proteins were bacterially expressed and purified, and emission spectra were measured; however, the BRET proteins with tdTomato were mostly insoluble.

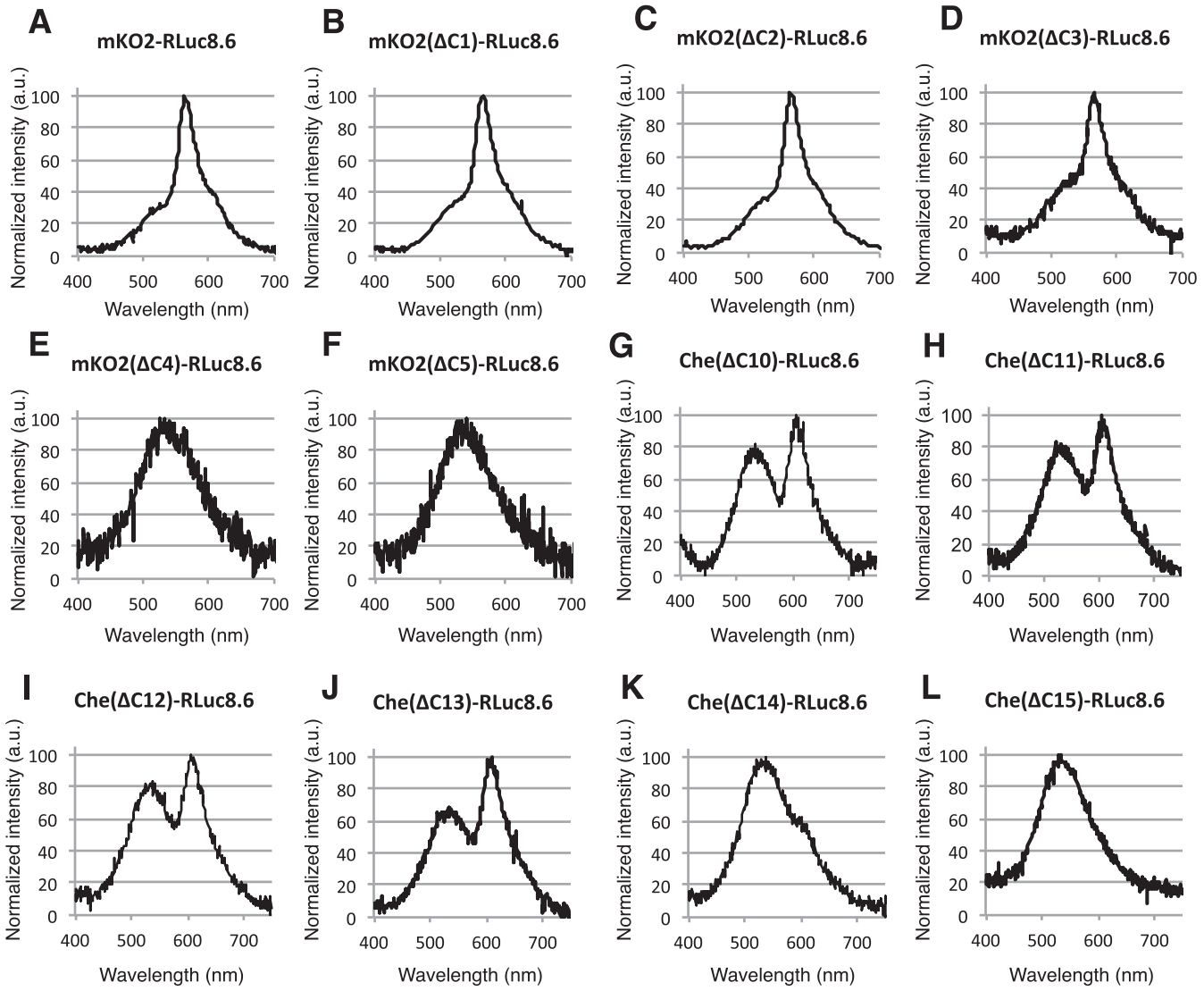

Fig. S3. Effects of deletions of the linker between RLuc and FP. (*A–F*) Emission spectra of BRET proteins based on mKusabiraOrange2-RLuc8.6. (*G–L*) Emission spectra of BRET proteins based on mCherry-RLuc8.6. BRET proteins were expressed in MDCKII cells, and emission spectra were measured with the cell lysates.

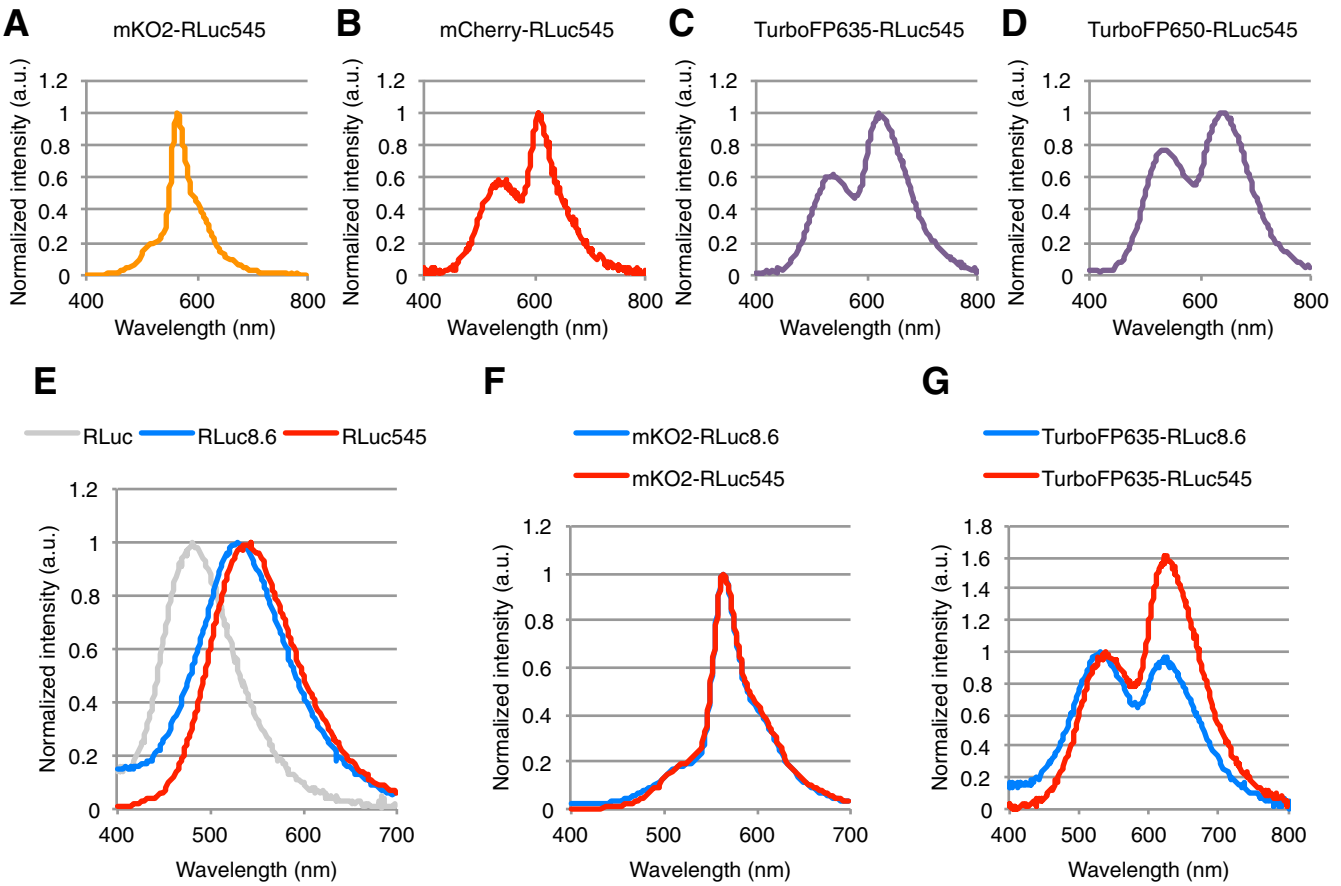

Fig. S4. Emission spectra of RLuc8.6–545-based BRET proteins. (*A–D*) Emission spectra of each BRET protein. (*E*) Differences of emission spectra in RLuc, RLuc8.6, and RLuc8.6–545 (presented as RLuc545). (*F*) Comparison of emission spectra between mKO2-RLuc8.6 and mKO2-RLuc545 (mKusabiraOrange2 was presented as mKO2). (*G*) Comparison of emission spectra between TurboFP635-RLuc8.6 and TurboFP635-RLuc545. Note the higher donor-to-acceptor ratio of TurboFP635-RLuc545; its emission peak is in the range of optical window for intravital imaging (600–1,000 nm).

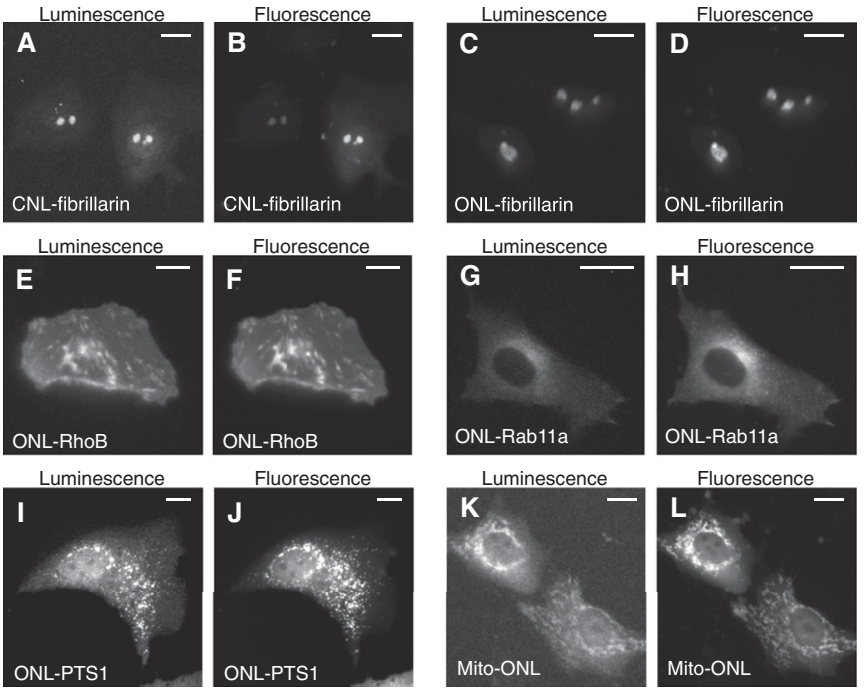

Fig. S5. Luminescence and fluorescence images of multicolor Nano-lanterns. Luminescence and fluorescence images of CNL and ONL in MDCKII cells: (*A* and *B*) CNL-fibrillarin (nucleoli), (*C* and *D*) ONL-fibrillarin (nucleoli), (*E* and *F*) ONL-RhoB (plasma membrane and endosomes), (*G* and *H*) ONL-Rab11a (recycling endosomes), (*I* and *J*) ONL-PTS1 (peroxisomes), and (*K* and *L*) Mito-ONL (mitochondria). Exposure times: luminescence images, 1–2 s; fluorescence images, 0.03–0.1 s. (Scale bars: 10 μm.)

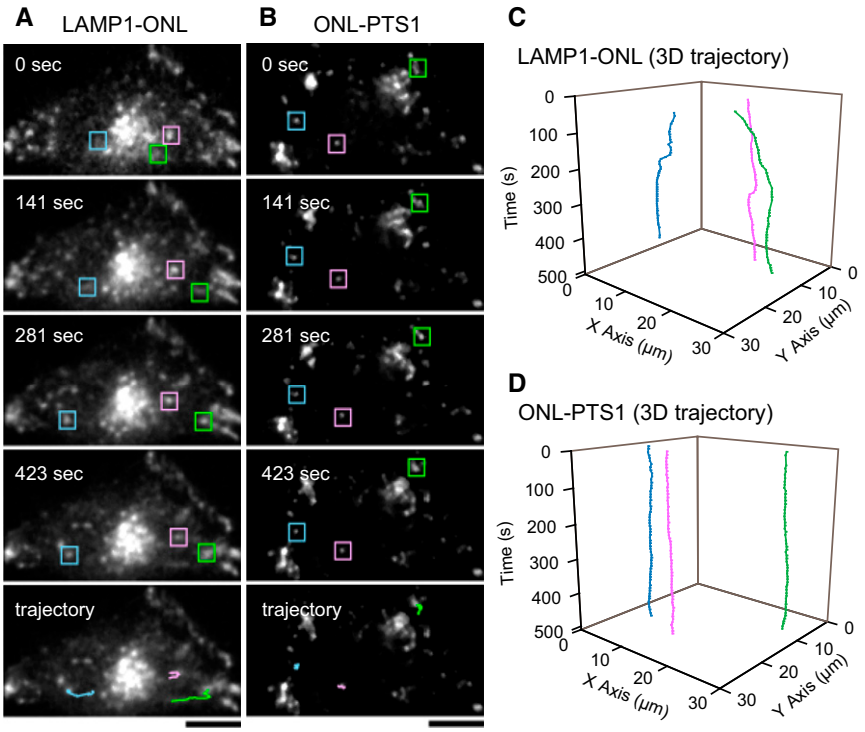

Fig. S6. Trajectory analysis of lysosomes and peroxisomes. (*A* and *B*) Luminescence imaging of the MDCKII cell expressing (*A*) LAMP1-ONL and (*B*) ONL-PTS1. (*C* and *D*) Trajectory analyses of (*C*) LAMP1-ONL and (*D*) ONL-PTS1. The positions of lysosomes and peroxisomes were determined by a 2D Gaussian fitting algorithm with custom software. Exposure times: *A*, 2 s; *B*, 3 s. (Scale bars: 10 μm.)

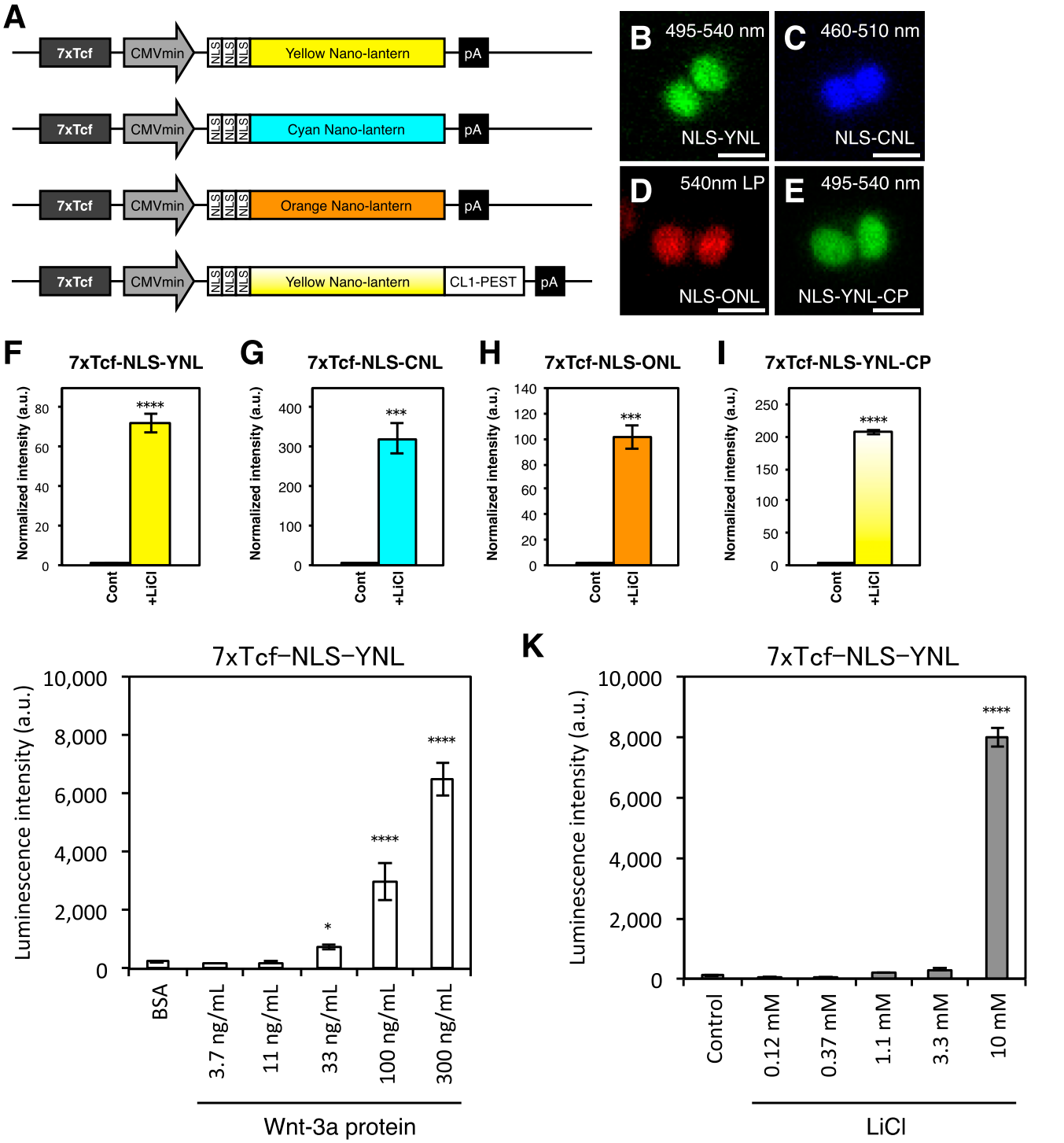

Fig. S7. Responsiveness of Wnt reporter cell lines. (*A*) Schematics of Wnt signal reporters based on multicolor Nano-lanterns. (*B–E*) Luminescence of NLS-tagged multicolor Nano-lanterns expressed in Wnt reporter HEK293A cell lines. Images were acquired with (*B* and *E*) 495- to 540-nm band-pass, (*C*) 460- to 510-nm band-pass, and (*D*) 540-nm long-pass emission filters at 16 h after the addition of 10 mM LiCl. Exposure times: 0.5 s. (Scale bars: 10 μm.) (*F–I*) Luminescent intensities in Wnt reporter HEK293A cell lines were measured at 16 h after the addition of 10 mM LiCl. Intensities were measured in triplicate, and data are presented as means ± SDs. Student's *t* test. ***$P < 0.001$; ****$P < 0.0001$. (*J* and *K*) Luminescence intensities of the 7xTcf-NLS-YNL stable line (HEK293A) at 16 h after addition of (*J*) BSA (control) or 3.7, 11, 33, 100, or 300 ng/mL Wnt-3a protein or (*K*) 0.12, 0.37, 1.1, 3.3, or 10 mM LiCl. Intensities were measured in triplicate, and data are presented as means ± SDs. One-way ANOVA followed by posthoc Tukey's honestly significant difference test compared with each control. *$P < 0.05$; ****$P < 0.0001$.

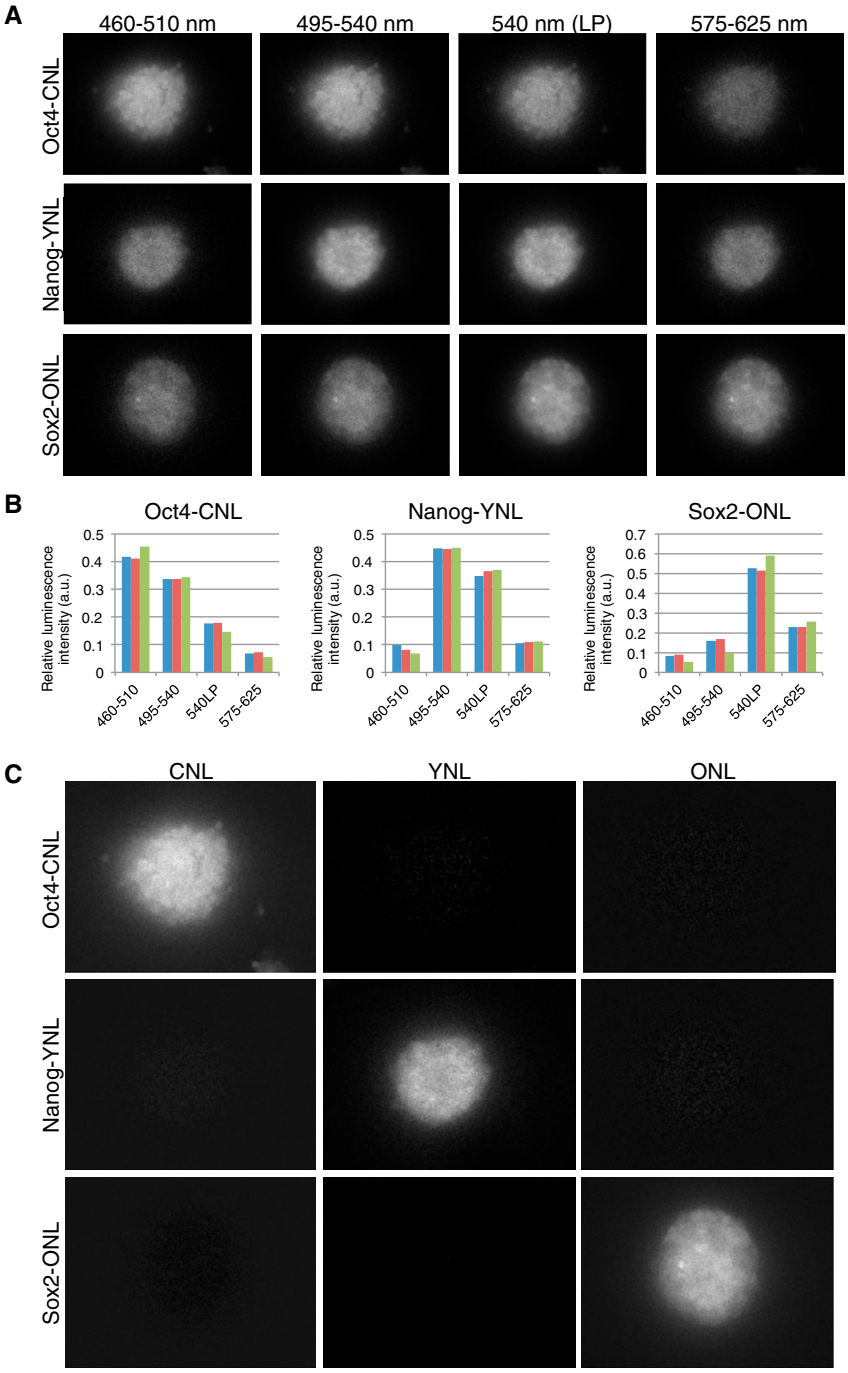

Fig. S8. Multicolor imaging with linear unmixing. (*A*) ES cells expressing CNL, YNL, or ONL were imaged with four filter conditions. (*B*) Linear unmixing coefficients were determined from the control experiments as in *A*. Blue bars show the values with a 40× objective, red bars show the values with a 100× objective, and green bars are the theoretical estimate from the spectrum of the Nano-lanterns and filters. (*C*) Proof for the separation with the images shown in *A*.

Table S1. Enzymatic characteristics of LPs

Name	QY (%)	K_m (μM)	V_{max} (photons × enzyme^{-1} × s^{-1})
RLuc	2.04 ± 0.0970	3.16 ± 0.570	0.0983 ± 0.00771
RLuc8.6	2.08 ± 0.169	2.26 ± 0.0544*	0.246 ± 0.00536†
YNL	14.0 ± 1.52†	1.90 ± 0.117‡	0.538 ± 0.0169†
CNL	14.3 ± 1.04†	1.35 ± 0.731§	0.882 ± 0.0264†
ONL	5.02 ± 0.361*	1.70 ± 0.102‡	0.785 ± 0.0153†

QYs and kinetic parameters of the LPs determined from the experiments shown in Fig. S1. All data were measured in triplicate, and data are presented as means ± SDs. One-way ANOVA followed by posthoc Tukey's honestly significant difference test compared with RLuc.

*$P < 0.05$.

$^{\dagger}P < 0.0001$.

$^{\ddagger}P < 0.01$.

$^{\S}P < 0.001$.

Table S2. Apparent BRET efficiencies of BRET protein

Name	$I_{acceptor}/I_{donor}$
RLuc8-S257G–based BRET constructs (Fig. S2)	
LSSmOrange(FL)-RLuc8-S257G	0.683
LSSmOrange(ΔC10)-RLuc8-S257G	0.774
mKeimaRed-RLuc8-S257G	0.115
tdTomato-RLuc8-S257G	2.36
mCherry-RLuc8-S257G	0.547
TurboFP635-RLuc8-S257G	0.173
mKate2-RLuc8-S257G	0.0959
RLuc8.6-based BRET constructs (Fig. S2)	
LSSmOrange(ΔC10)-RLuc8.6	1.50
mKeimaRed-RLuc8.6	0.350
tdTomato-RLuc8.6	4.49
mCherry-RLuc8.6	1.34
TurboFP635-RLuc8.6	0.522
mKate2-RLuc8.6	0.442
mOrange2-RLuc8.6	1.38
TagRFP-RLuc8.6	1.23
mKusabiraOrange2-RLuc8.6 (ONL)	4.76
mRuby-RLuc8.6	1.36
mKO2- and mCherry-based BRET constructs (Fig. S3)	
mKusabiraOrange2(ΔC1)-RLuc8.6	2.74
mKusabiraOrange2(ΔC2)-RLuc8.6	2.78
mKusabiraOrange2(ΔC3)-RLuc8.6	2.09
mKusabiraOrange2(ΔC4)-RLuc8.6	0.864
mKusabiraOrange2(ΔC5)-RLuc8.6	0.868
mCherry(ΔC11)-RLuc8.6	1.14
mCherry(ΔC12)-RLuc8.6	1.17
mCherry(ΔC13)-RLuc8.6	1.40
mCherry(ΔC14)-RLuc8.6	0.550
mCherry(ΔC15)-RLuc8.6	0.396
RLuc8.6–545-based BRET constructs (Fig. S4)	
mKusabiraOrange2-RLuc8.6–545	2.92
mCherry(ΔC13)-RLuc8.6–545	1.69
TurboFP635(ΔC10)-RLuc8.6–545	1.57
TurboFP650(ΔC10)-RLuc8.6–545	1.28

Comparison of BRET efficiency of BRET proteins shown in Figs. S2–S4. Here, we report the ratio of luminescent intensities of the acceptor peak ($I_{acceptor}$) to that of the donor peak (I_{donor}) as the quick measure for the BRET efficiency. Note that tdTomato-fusion proteins had the problem of solubility.

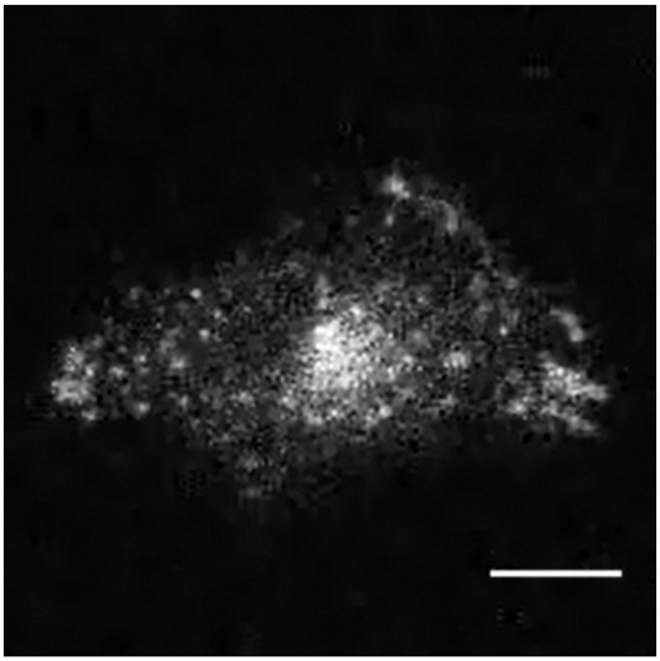

Movie S1. Continuous luminescence imaging of LAMP1-ONL in an MDCKII cell. Images with 2-s exposure were repeated for 7.8 min. Playback speed is 200-fold. (Scale bar: 10 μm.)

Movie S1

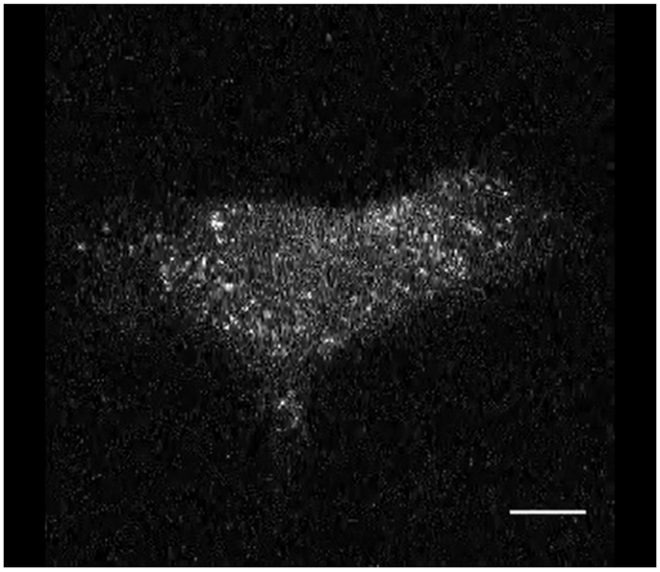

Movie S2. Continuous luminescence imaging of ONL-PTS1 in an MDCKII cell. Images with 3-s exposure were repeated for 8.8 min. Playback speed is 200-fold. (Scale bar: 10 μm.)

Movie S2

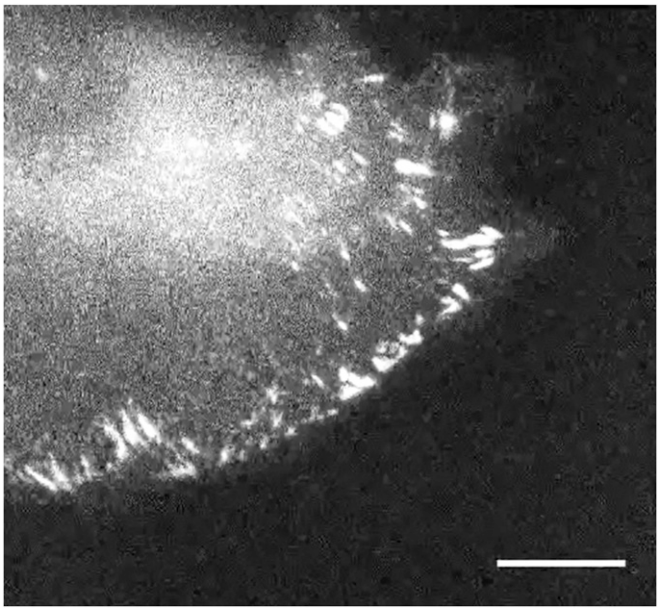

Movie S3. Long-term continuous luminescence imaging of vinculin-ONL in an MDCKII cell. Images with 1-s exposure were repeated for 240 min. Playback speed is 6,000-fold. (Scale bar: 10 μm.)

Movie S3

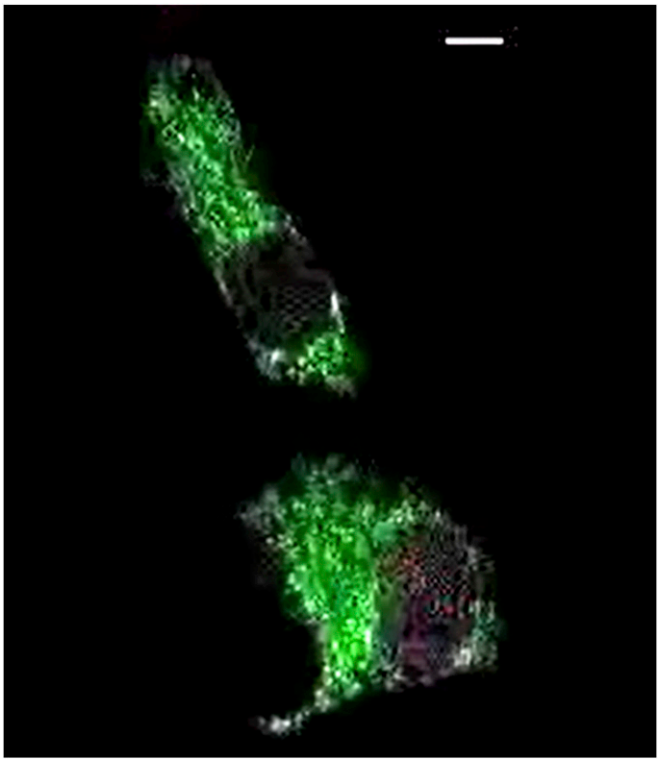

Movie S4. Dual-color luminescence imaging of Ca^{2+} indicators. Time-lapse dual-color luminescent imaging of Mito-CNL(Ca^{2+}) and ONL(Ca^{2+})-H2B in HeLa cells. Images of each color were acquired simultaneously using W-View equipped with 550-nm long- and short-path filters for 7.5 min at the rate of 1 frame per 1 s; 20 μM histamine was added at 45 s after the start of imaging. Playback speed is 30-fold. (Scale bar: 10 μm.)

Movie S4